


Pretransitional short-range ordering in a triangular lattice of Ising spin chains

V. Hardy,* V. Caignaert, O. Pérez, L. Hervé, N. Sakly, and B. Raveau
Laboratoire CRISMAT, UMR 6508, CNRS, 6 Boulevard Maréchal Juin, 14050 Caen Cedex, France

Md. M. Seikh
Department of Chemistry, Visva-Bharati, Santiniketan-731235, West Bengal, India

F. Damay
Laboratoire Léon Brillouin, CEA Saclay, CNRS UMR12, F-91191 Gif-sur-Yvette, France

 (Received 10 July 2018; published 9 October 2018)

$\text{Sr}_2\text{Ca}_2\text{CoMn}_2\text{O}_9$ is made of Ising spin chains distributed on a triangular lattice, with antiferromagnetic coupling between them. In spite of a unique interchain distance, this compound exhibits two peculiarities making it deviate from the textbook case of geometrical frustration expected in ideal triangular lattices: first, there are three subclasses of chains shifted from each other along the chain direction; second, these chains fall into two categories which differ by some of the intrachain distances between spins. These features are found to confer a character of centered honeycomb lattice on this system of spin chains. Experimental investigation of the magnetism of $\text{Sr}_2\text{Ca}_2\text{CoMn}_2\text{O}_9$ reveals a peculiar pretransitional regime, which is manifested by a frequency-dependent peak of susceptibility. We put this behavior in relation with the formation of short-range one-dimensional ferromagneticlike segments taking place a few degrees above the T_N . This phenomenon is itself regarded as a precursor effect of the long-range ordering, induced by the particular topology of the spin system.

DOI: [10.1103/PhysRevB.98.144414](https://doi.org/10.1103/PhysRevB.98.144414)

I. INTRODUCTION

Geometrical frustration (GF) is a long-standing issue in magnetism, which is also often used as a prototypical illustration of the role of entropy in statistical physics [1]. In simple words, GF corresponds to the inability for a spin system to find a structure fully satisfying all the interaction links at the same time. The reasons for such a situation are only related to the topology of the links combined with the signs of the couplings. For GF, not only disorder is useless, but it rather tends to blur the specific manifestations of this type of frustration.

The most famous situation of GF takes place in two dimensions (2D), when considering a perfect triangular lattice with antiferromagnetic coupling between Ising spins [1,2]. Most of the theoretical works have dealt with pure 2D lattices [3], while real-life materials are by essence 3D, which requires the introduction of some interlayer coupling. As long as this interaction remains weak, one is dealing with the so-called stacked-triangular-lattice models, but, at the other limit, when this perpendicular coupling becomes the predominant one, a more relevant description is that of spin chains lying on a triangular lattice.

The archetypical example of this latter situation is the ABX_3 family (A being an alkali metal, B a transition metal, and X a halogen) [4]. Some of these compounds are made of Ising spins (e.g., CsCoCl_3 or CsCoBr_3) [5], and they were involved in the development of the concept of partially

disordered antiferromagnetic (PDA) state [6]: This is a long-range magnetic order associated with antiferromagnetic (AF) interchain coupling, in which two-thirds of the chains are AF coupled, while the last third is made of incoherent chains, i.e., along which the spins randomly vary between \uparrow and \downarrow to keep a zero net magnetization.

The $2H$ -perovskite related oxides constitute another family of spin chains on triangular lattices which has received increasing attention since the end of the 1990s [7]. The chains in these compounds are made of a stacking of face-sharing trigonal prisms (TP) and octahedra (Oh). It is a huge family, structurally more complex and varied than the ABX_3 since numerous stacking motifs between TP and Oh can be stabilized [8]. The simplest configuration is found in the compounds of formulation $A_3A'BO_6$ showing a regular alternation 1TP-1Oh (hereafter referred to as the “ O_6 ”). This subclass has been the most widely investigated so far, in particular those compounds showing an Ising character associated with the presence of cobalt on the TP, such as $\text{Ca}_3\text{Co}_2\text{O}_6$ [9,10], $\text{Ca}_3\text{CoRhO}_6$ [11,12], and $\text{Ca}_3\text{CoMnO}_6$ [13].

To date, the subclass of formulation $A_4A'B_2O_9$ (referred to as “ O_9 ”), made of repeating units 1TP-2Oh, has attracted less attention [14,15]. Recently, we have reinvestigated the compound $\text{Sr}_4\text{CoMn}_2\text{O}_9$ motivated by the puzzling spin dynamics reported by Boulahya *et al.* [16]. This compound exhibits a marked Ising character and does not show any sign of long-range ordering (LRO). Analysis of the dc and ac susceptibilities led us to interpret the dynamical response in terms of blocking effects, involving either the chains or the Co^{2+} themselves [17]. Both mechanisms were placed in relation with generic behaviors usually reported in

*vincent.hardy@ensicaen.fr

molecular compounds, i.e., single-chain magnet (SCM) [18] and single-ion magnet (SIM) [19], respectively. Making use of chemical pressure effects, progressive substitution of Ca for Sr was carried out to increase the interchain coupling. Such $\text{Sr}_{4-x}\text{Ca}_x\text{CoMn}_2\text{O}_9$ compounds were obtained for x up to 2.7, and it was found that LRO emerges for $x \geq 1.5$, leading to a disappearance of SCM but a persistence of SIM signatures [20].

The present paper aims at providing a closer look at this LRO. By combining samples of improved chemical homogeneity, additional experimental techniques, and increased resolution in temperature, it is shown that the transition is actually made of two closely spaced features. We found that this splitting can be regarded as a short-range ordering (SRO) taking place a few kelvin above the LRO. The study was performed in $\text{Sr}_2\text{Ca}_2\text{CoMn}_2\text{O}_9$, for which these two features are separated by about 4 K. This is a type of precursor effect in the magnetic transition of spin-chain compounds.

II. EXPERIMENTAL DETAILS

The $\text{Sr}_2\text{Ca}_2\text{CoMn}_2\text{O}_9$ samples were synthesized by standard solid-state reaction from stoichiometric mixtures of CaCO_3 , SrCO_3 , Co_3O_4 , and MnO , following a previously described procedure [17]. The chemical homogeneity and crystallinity of these compounds are highly sensitive to the intermediate grinding/heating steps, as well as to the final heating conditions. For the samples used in the present study, intermediate grindings and heatings at 1000 °C for 24 h were repeated three times. Care was also taken to ensure that the last sintering step took place at high enough temperature and for long enough time (1250 °C and 40 h, respectively) to yield excellent crystallinity (see Supplemental Material [21]). The cationic ratio was determined from energy-dispersive spectroscopy using an analyser Link ISIS mounted on an electron microscope (Oxford Instruments).

Powder x-ray diffraction (PXRD) patterns were registered with a Panalytical X'Pert Pro diffractometer under a continuous scanning mode in the 2θ range 10° – 120° and step size $\Delta(2\theta) = 0.017^\circ$ with $\text{Cu K}\alpha$ radiation. Powder neutron-diffraction (PND)-experiments were carried out with the high-resolution powder diffractometer HRPT at Paul-Scherrer-Institute (PSI, Villigen), using $\lambda = 1.494 \text{ \AA}$ [Ge(533)]. Additional PND experiments were conducted at Laboratoire Léon Brillouin (LLB, CEA-Saclay) to investigate the magnetic structure. These experiments were carried out on the powder diffractometer G 4.1 using $\lambda = 2.426 \text{ \AA}$, at 25 temperatures between 300 and 2 K. The structural characterization was carried out by combining PXRD and PND data recorded at room temperature. The refinements of the atomic positions (see Supplemental Material [21] for all the crystallographic data) were obtained in the frame of a multidimensional approach developed for aperiodic systems (see Ref. [17] for details of the procedure).

Specific heat measurements were carried out in a Physical Properties Measurements System (PPMS, Quantum Design), by using a relaxation method with a $2\text{-}\tau$ analysis. The dc magnetization measurements were recorded using a superconducting quantum interference device magnetometer (MPMS, Quantum Design). ac susceptibility measurements were

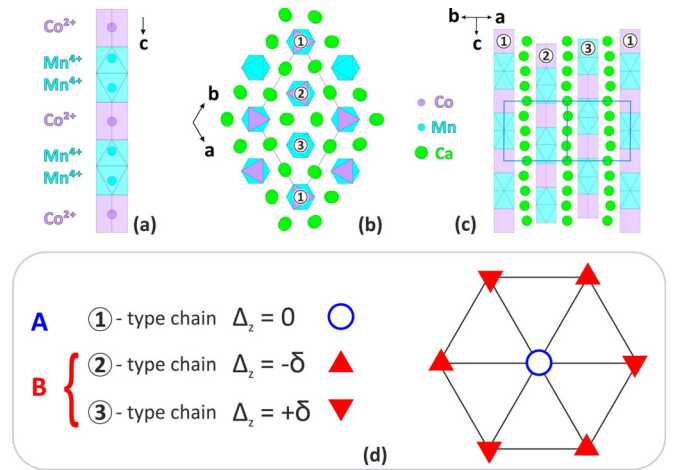


FIG. 1. (a) Side view of the type of spin chains encountered in $\text{Sr}_2\text{Ca}_2\text{CoMn}_2\text{O}_9$. They are made of a regular stacking of face-sharing octahedra (hosting Mn^{4+}) and trigonal prisms (hosting Co^{2+}) in a ratio 2:1. (b) Perpendicular view showing the triangular arrangement of these chains, separated by columns of randomly mixed Sr^{2+} and Ca^{2+} (green circles). Also highlighted is the presence of three subclasses of chains (labeled 1 to 3), which are in equal proportions. Panel (c) exhibits the offset present (along the c axis) between neighboring chains. There is also an intrinsic difference between the chains 1 for which there is a unique nn Co-Mn interdistance (A family) and the chains 2 and 3 (B family) which contain two Co-Mn spacings (see text). As schematically shown in panel (d), if the chains A are taken as a reference for the z coordinate ($\Delta_z = 0$), the B chains are shifted by $\delta \sim 1.9 \text{ \AA}$ in two opposite directions. The spatial arrangement between the A and B chains on the triangular lattice is also displayed.

conducted in the MPMS and in the PPMS, using in both cases an excitation field equal to $h_{ac} = 10 \text{ Oe}$. Aggregating data from these two devices allows covering a broad range of frequency (10^{-1} – 10^4 Hz). Harmonics of the ac susceptibility were also investigated in the PPMS. Considering an excitation field in the form $h(t) = h_{ac}\cos(\omega t)$, the general magnetic response can be written as $M(t) = \sum_{n=1}^{\infty} \chi_{n\omega} h_{ac} \cos(n\omega t + \varphi_n)$. We have considered in the present study the amplitude of the second and third harmonics, i.e., $\chi_{2\omega}$ and $\chi_{3\omega}$. Having a residual field as low as possible is crucial to get reliable “zero-field” data. In devices hosting superconducting coils (5 and 9 T for MPMS and PPMS, respectively) pinned vortices can generate a nonzero remanent field. Even after proper demagnetizing procedures, this H_{rem} cannot be decreased below about +1.5 and +4 Oe in the MPMS and PPMS, respectively. Zero-field measurements were thus recorded by applying a compensation field $H_{\text{comp}} = -H_{\text{rem}}$ to get a residual field that should be limited to values similar to earth’s field.

III. STRUCTURAL FEATURES

The spin chains in $\text{Sr}_2\text{Ca}_2\text{CoMn}_2\text{O}_9$ are made of face-sharing TP (hosting the Co^{2+}) and Oh (hosting the Mn^{4+}), stacked in a regular sequence of 1 TP for 2 Oh [Fig. 1(a)]. These chains are distributed on a triangular lattice, and columns made of a random mixture of Sr^{2+} and Ca^{2+} are located between them [Fig. 1(b)]. The situation is complexified

by two important features. First, there are three subclasses of chains, which differ by relative shifting along the c axis (chain direction). The spatial arrangement of these subclasses (labeled 1, 2, and 3) is shown in Figs. 1(b) and 1(c). Such shiftings between neighboring chains are a common feature of all the compounds of the “2H” family, which has already attracted attention in the O_6 compounds [22]. Second, all the chains are not strictly equivalent when considering the intercationic distance: there is a unique Co-Mn distance in chains 1 ($d = 2.62$ Å), whereas chains 2 and 3 exhibit an alternation between long and short Co-Mn spacings (denoted $d_L = 2.78$ Å and $d_S = 2.48$ Å, respectively) [17]. The former category will be referred to as the A chains and the latter as the B chains. Such an intrinsic difference between chains (beyond relative offsets in their positioning along the c axis) was not reported in the O_6 family. Note that the difference between the two categories of chains in $\text{Sr}_2\text{Ca}_2\text{CoMn}_2\text{O}_9$ deals almost exclusively with the Co-Mn distances, while the Co-Co and Mn-Mn spacings along the c axis remain virtually identical in all the chains ($d_L + d_S \cong 2d$). Adopting the A chains (subclass 1) as a reference for the relative positioning along the c axis, one observes that half of the B chains (subclass 2) are shifted downward by $-\delta$ while the second half (subclass 3) are shifted upward by $+\delta$, with $\delta \sim 1.9$ Å [Fig. 1(d)].

The spin chains of $\text{Sr}_2\text{Ca}_2\text{CoMn}_2\text{O}_9$ present an Ising-like character originating from the strong easy-axis character of Co^{2+} in the TP environment [23]. This feature has been quantified by a single-ion anisotropy parameter D on the order of -150 K when considering an energy of the form $D(S^2 - 1/4)$ (with $S = 3/2$) [24]. In terms of interaction energies, the structure of face-sharing polyhedra imposes to consider at least the next-nearest neighbors (nnn) in addition to nearest neighbors (nn) for the intrachain couplings. It means that at least four couplings have to be taken into account, as shown in Fig. 2(a): J_1 between nn Mn-Mn, J_2 between nn Co-Mn, J_3 for nnn Mn-Mn, and J_4 for nnn Co-Mn. If all these interaction are AF, their competition yields magnetic frustration. Despite the lack of information about J_4 , estimates of J_1 , J_2 , and J_3 derived from previous studies on related compounds [14,25] indicate that one is facing such a situation of frustration. In a previous study, we found that the best compromise in terms of energy is obtained with an arrangement $\uparrow\downarrow\uparrow$ along each Co-Mn-Mn unit [17].

As in all the 2H-perovskite related oxides, the interchain coupling is AF, with an intensity about two orders of magnitude lower than for the intrachain couplings. Even though there is a unique interchain distance $d^* = 5.41$ Å, the presence of the three subclasses of chains leads to departure from the ideal situation of GF associated with standard triangular lattice. First, the difference in the Co-Mn distances between the A and B chains [Fig. 2(c)] must impact the associated couplings (i.e., J_2 and J_4), in such a way that $\text{Sr}_2\text{Ca}_2\text{CoMn}_2\text{O}_9$ should be regarded as a centered honeycomb lattice rather than as a pure triangular one [Fig. 2(b)]. Second, the shifting along c between neighboring chains also contributes to deviate from an ideal triangular lattice. In $\text{Sr}_2\text{Ca}_2\text{CoMn}_2\text{O}_9$ the relative shift is $|\delta|$ for interaction A-B, whereas it is $|\delta|$ for B-B. Eventually, one has to distinguish two types of nn interchain couplings: j_{AB} and j_{BB} [see Fig. 2(b)].

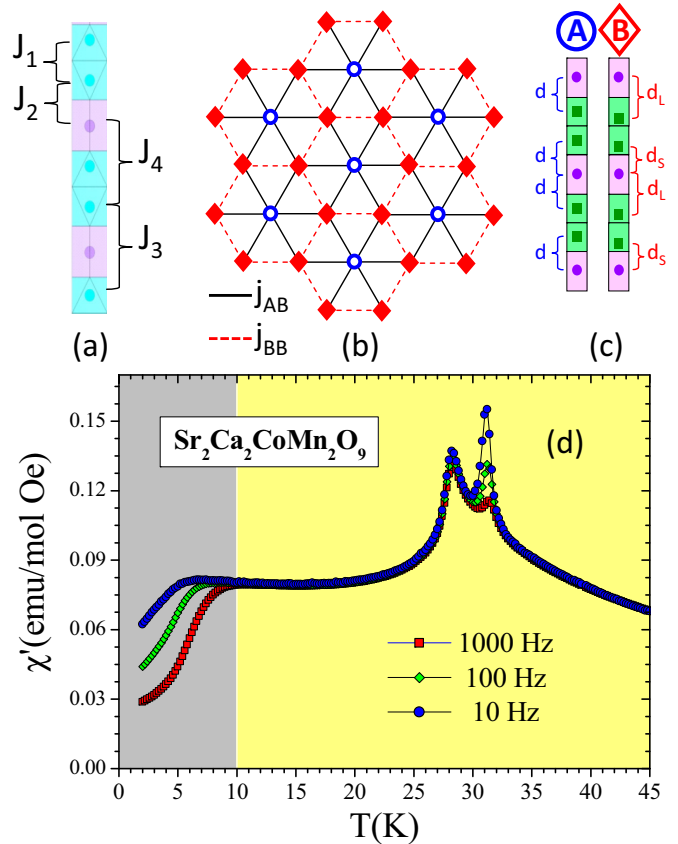


FIG. 2. Panel (a) shows the four nn- and nnn intrachain couplings that have to be taken into account (Mn⁴⁺ and Co²⁺ occupy the cyan and magenta polyhedra, respectively). (b) Perpendicular view showing the regular arrangement of the A and B chains over a large scale, as well as the two types of nn interchain couplings that are encountered. Panel (c) focuses on the intrinsic difference between the A and B chains, which can be regarded as a central or noncentral positioning of the Mn₂ pairs in between two consecutive Co. This yields only one Co-Mn interdistance for A (denoted d), whereas there is a regular alternation between short and long bonds for B (d_S and d_L , respectively). Panel (d) shows the in-phase ac susceptibility at three frequencies. The gray-shaded area corresponds to the regime of slow spin dynamics previously discussed in terms of single-ion magnetism [17].

IV. PHYSICAL PROPERTIES

Figure 2(d) shows the ac susceptibility of $\text{Sr}_2\text{Ca}_2\text{CoMn}_2\text{O}_9$ over a broad range of temperature, at three selected frequencies. The regime of slow spin relaxation at lowest temperatures (gray-shaded area) was previously ascribed to a behavior of SIM [17,20]. The present paper focuses on the regime at higher temperature (yellow-shaded area) around the T_N . The broad peak previously reported at T_N is actually found to be split into two features separated by about 4 K. Figure 3 shows an enlargement of the double-peaks regime with frequencies spanning five orders of magnitude. About the peak at lower T , one observes that its position is virtually frequency independent, while its height is somewhat decreased as frequency increases. The T_N previously reported for $\text{Sr}_2\text{Ca}_2\text{CoMn}_2\text{O}_9$ can be associated with this first peak [17]. The amplitude of

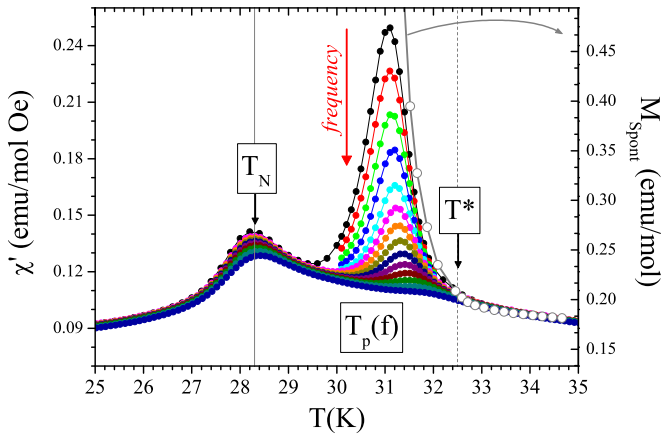


FIG. 3. Enlargement of the temperature range showing the double-peak structure. In-phase ac susceptibility curves are shown for 14 frequencies between 10^{-1} and 10^4 Hz. The spontaneous magnetization measured upon cooling in a dc field of ~ 1.5 Oe is also shown (right axis). The solid line corresponds to the center of the low- T peak (virtually frequency independent) which is ascribed to an antiferromagnetic transition (T_N). The dashed line corresponds to the rise of spontaneous magnetization (T^*). The frequency-dependent peaks of χ'' [denoted $T_p(f)$] take place between T_N and T^* .

the second peak is much more impacted by the frequency, in such a way that it is dominant at 10^{-1} Hz, whereas it becomes hardly detectable at 10^4 Hz. Note that the position of this peak, hereafter denoted as $T_p(f)$, slightly shifts toward higher temperature as the frequency is increased, an issue that will be addressed in more detail below. Figure 3 also displays the spontaneous magnetization (M_{spont}) that was recorded upon cooling in a field of ~ 1.5 Oe. This curve exhibits an abrupt divergence from the paramagneticlike response around 32.5 K, a temperature that will be referred to as T^* .

Figure 4 shows the temperature dependence of three quantities expected to reflect the onset of a magnetic ordering, namely the magnetization (presented in the form of dc susceptibility $\chi_{\text{dc}} = M/H$), the heat capacity (C), and the intensity of PND peaks. In each panel the positions of T_N and T^* are indicated. First of all, one observes that these data confirm the achievement of LRO at T_N , since this temperature corresponds well to the inflection point on the high- T side of a peak in $C(T)$, as well as to the rise of peak intensities in PND. There is also a change in M at T_N , which depends on the field value: in low field, M exhibits a steep increase at T_N upon cooling, whereas it shows a peak in higher field. As for T^* , there is no detectable feature in C nor in PND (within experimental uncertainty). In other respects, T^* is clearly correlated to the first rise of M in low field (10^2 Oe), in line with the behavior observed for M_{spont} . When increasing the magnetic field (10^4 Oe), no signature of T^* can be detected.

The transitional regime encompassing T_N and T^* is investigated in more detail in Fig. 5. Besides the influence of the field value, panel (a) addresses the hysteretical nature of the magnetic response, as well as the connection between the ac and dc susceptibilities. In low-dc field (10 Oe) the sharp upturn in χ_{dc} below T^* is followed by a “plateaulike” regime (in log scale) before reincreasing at T_N . Note that the

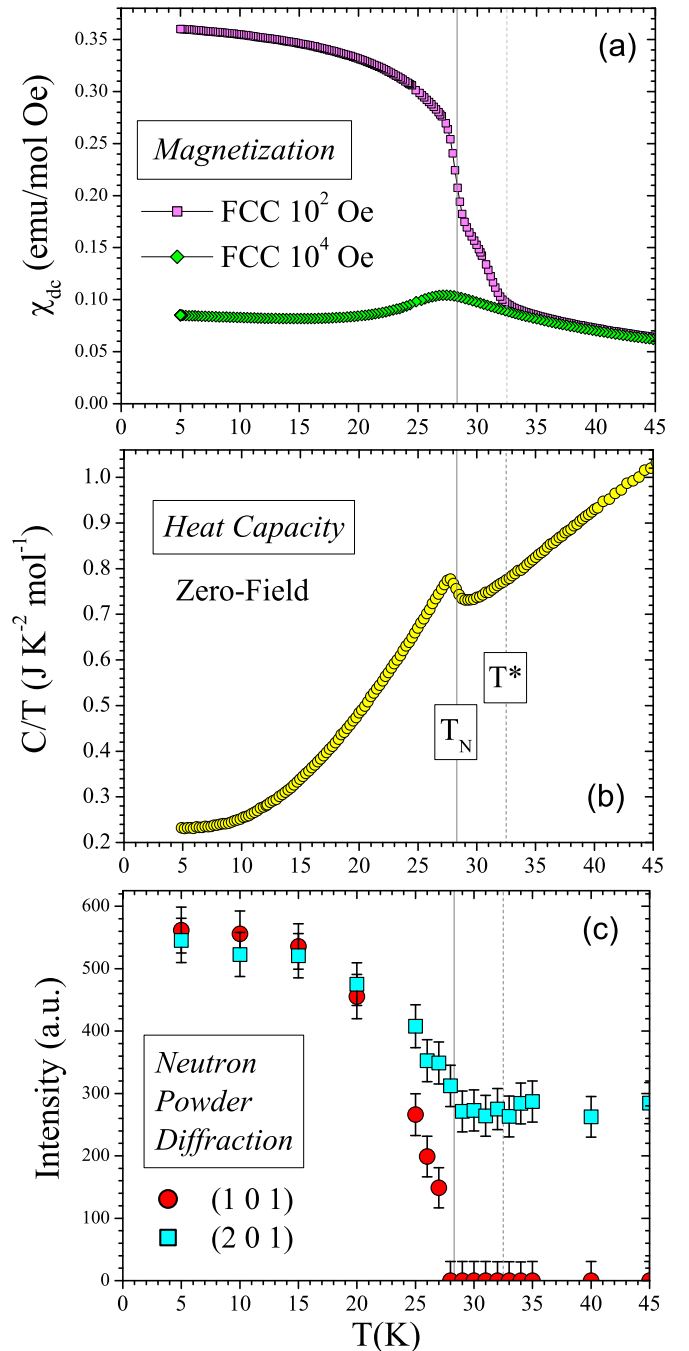


FIG. 4. Temperature dependence of several bulk properties in $\text{Sr}_2\text{Ca}_2\text{CoMn}_2\text{O}_9$. The solid and dashed lines correspond to T_N and T^* , respectively (see Fig. 3). Panel (a) shows dc magnetization measured in “low”- and “high”-field values, using the field-cooled-cooling procedure. Panel (b) shows the heat capacity measured in zero field, and (c) the intensity of two magnetic peaks typical of the PDA structure (see text), with vertical bars representing the experimental uncertainty. Note that the underlying nuclear intensity is very weak for (101) contrary to (201).

hysteresis between ZFC and FCC branches (zero-field-cooled and field-cooled-cooling, respectively) does not start at T^* , but rather at the high- T side of the plateau. When increasing the field, no signature of T^* is visible (even in a moderate field of

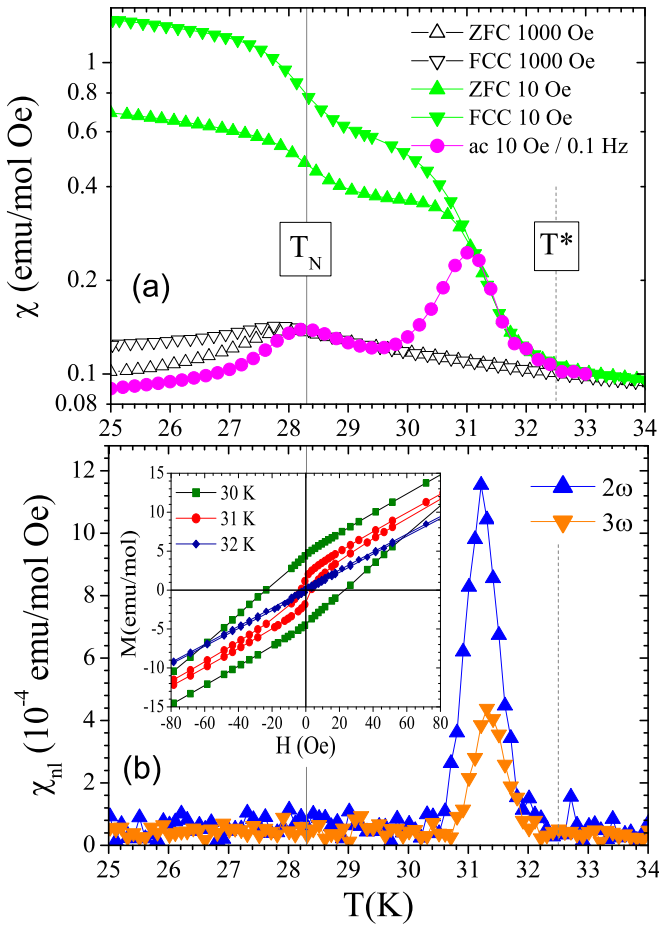


FIG. 5. Panel (a) is an enlargement of susceptibility curves within the double-peak regime, showing dc response (M/H) measured with zero-field-cooled or field-cooled cooling procedures, for two field values, as well as ac susceptibility measured at our lowest frequency of 0.1 Hz. Panel (b) shows the second and third harmonics, measured at 46 Hz. The inset displays isothermal hysteresis loops recorded after zero-field cooling.

10^3 Oe) and hysteresis only starts developing below the peak at T_N . It can be noted that our lowest frequency of 10^{-1} Hz corresponds to a time constant approaching that of dc measurements. Around T^* , one observes a good superimposition of the ac data recorded at this frequency (with $h_{ac} = 10$ Oe) onto the dc data measured in $H = 10$ Oe. Upon cooling, the ac susceptibility first exhibits a peak centered at the temperature where hysteresis appears for dc data, before showing a second peak at T_N .

Figure 5(b) shows the second and third harmonics of the ac susceptibility. Both for $\chi_{2\omega}$ and $\chi_{3\omega}$, one observes a sharp peak having a full width at half maximum less than 1 K. These peaks emerge at about 32 K, in close agreement with that of the first harmonic [see panel (a)], i.e., at a temperature just below T^* [26]. No feature can be detected at T_N for both $\chi_{2\omega}$ and $\chi_{3\omega}$, at any frequency. The data shown for the harmonics correspond to the lowest frequency presenting acceptable signal-to-noise ratio (46 Hz). Actually, the peaks in $\chi_{2\omega}$ and $\chi_{3\omega}$ are discernible down to the lowest investigated frequency (10 Hz), while they progressively disappear when

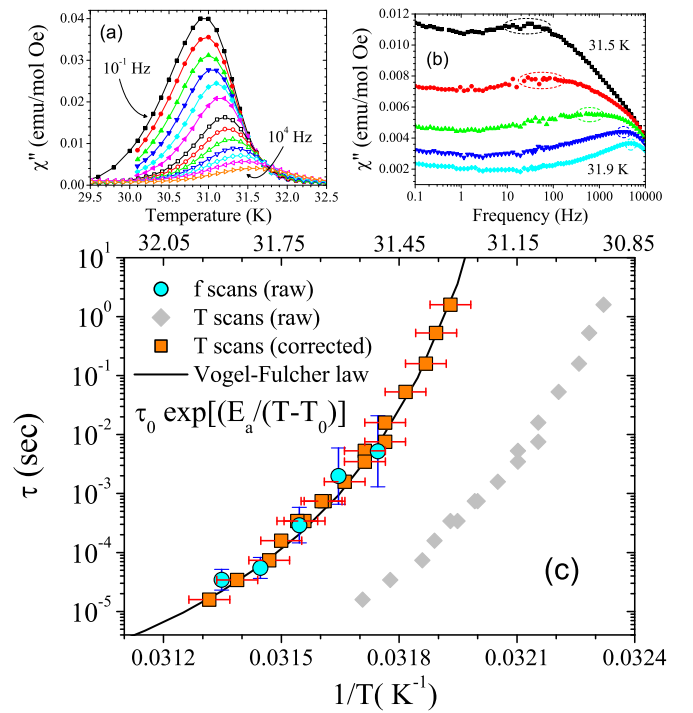


FIG. 6. Out-of-phase susceptibility within the $T_p(f)$ regime, measured either (a) versus temperature at fixed frequencies (logarithmically spaced values), or (b) versus frequency at fixed temperatures (0.1 K steps). Panel (c) shows, in an Arrhenius plot, the temperature dependence of the spin-relaxation time derived from these data (see text). The solid line is a fitting by a Vogel-Fulcher law (see text).

frequency is increased above about 10^3 Hz. It must be noted that the presence of a peak in $\chi_{2\omega}(T)$ lends further support to the existence of a spontaneous magnetization [27]. As for the presence of a peak in $\chi_{3\omega}(T)$, this is often ascribed to a spin-freezing phenomenon, especially when this peak takes a sharp and symmetrical shape, as it is presently observed [27]. It can also be noted that the concomitant observation of both signatures is generally regarded as being indicative of a cluster-glass behavior [27]. The inset of Fig. 5(b) shows $M(H)$ loops recorded at several temperatures just below T^* . At 32 K, one observes an almost linear response without significant hysteresis; at 31 K, the $M(H)$ curve gets an S shape that is consistent with a ferromagneticlike component (showing remanent magnetization and coercive field) superimposed on a linear-in-field (paramagnetic) background; decreasing further T down to 30 K leads to a substantial opening of the loop. We note that the steep slope of the $M(H)$ at very low field (< 10 Oe) for $T = 31$ K is in accordance with the sharp upturn observed in the susceptibility curves below T^* [Fig. 5(a)].

Let us now turn back to the frequency dependence of the peak in $\chi'(T)$ at T_p , which was detected in Fig. 3. We consider hereafter the temperature dependence of the characteristic spin-relaxation time associated with this peak. For this purpose, we adopt the usual method based on the position of the peaks of $\chi''(f, T)$, using both measurements recorded versus temperature (T) at fixed frequency or versus frequency (f) at fixed temperatures (see Fig. 6). The $\chi''(T)$ data display well-defined peaks, whose location clearly shifts

toward higher temperature as frequency is increased, while their amplitude is decreased [Fig. 6(a)]. This contrasts with the $\chi''(f)$ data, for which one rather observes quite broad bumps and, furthermore, only within a narrow range of temperature [Fig. 6(b)]. Within the framework of a generalized Debye model (including a certain width in the distribution of the relaxation times), the out-of-phase susceptibility can be written as

$$\chi''(T, f) = \frac{(\chi_T - \chi_S)}{2} \frac{\cos\left(\frac{\alpha\pi}{2}\right)}{\cosh[(1-\alpha)\ln(2\pi f\tau_c)] + \sin\left(\frac{\alpha\pi}{2}\right)}, \quad (1)$$

where χ_T and χ_S are the isothermal and adiabatic susceptibilities, respectively, τ_c is the central value of the distribution of relaxation times, and α is a parameter reflecting its width [28]. Considering that a maximum in χ'' is mainly driven by the minimization of the denominator in the second term of Eq. (1), it is customary to derive τ_c from the relationships: $\tau_c(T_{\max}) = 1/(2\pi f)$ for the T scans, or $\tau_c(T) = 1/(2\pi f_{\max})$ for the f scans. Doing so was found to yield some inconsistency between the data derived from each type of measurement [29]. In fact, while this approach is correct for the f scans, it is not for the T scans since the prefactor in the right-hand-side of Eq. (1) is basically temperature dependent. To correct the analysis of the T scans, we followed a procedure (see Supplemental Material [21]) whose central part is to consider the location of the maximum of the quantity $\chi''(T)/[\chi_T(T) - \chi_S(T)]$, by using experimental approximations of $\chi_T(T)$ and $\chi_S(T)$. The final $\tau_c(T)$ obtained from both f - and T scans are shown in Fig. 6(c). For the f scans, the main source of uncertainty is directly connected to the identification of the maxima; the shown error bars thus correspond to the width of the ellipses in Fig. 6(b). For the T scans, the positions of the peaks are well defined, in such a way that the error bars shown just correspond to half the spacing between data points, i.e., ± 0.05 K.

The characteristic spin-relaxation time associated with the peak in ac susceptibility located above T_N varies very rapidly as a function of the temperature. Its divergence as T is decreased is much more pronounced than expected for a standard Arrhenius process [that would lead to a straight line in Fig. 6(c)]. The observed $\tau(1/T)$ shape is rather suggestive of a Vogel-Fulcher (VF) function, a phenomenological law often used to account for activation processes in the presence of interactions [30]. This law reads $\tau = \tau_0 \exp\left[\frac{E}{T-T_0}\right]$, where τ_0 is a microscopic attempt time, E the height of an energy barrier (here expressed in kelvin), and T_0 a characteristic temperature reflecting the intensity of the interactions between the spin units at play in the activation process. The solid line in Fig. 6(c) is the best fitting to the data obtained without assumption on any of the parameters. It leads to $\tau_0 \sim 10^{-9}$ s, $E \sim 11$ K, and $T_0 \sim 30.8$ K. It must be kept in mind that there is strong interdependence between the three parameters of a VF law, inducing sizable uncertainties in their determinations. With the present data, however, T_0 is quite well defined, allowing us to make the following remarks: First, T_0 lies in between T_N (28.3 K) and T^* (32.5 K); Second, when considering $T(\tau)$ from Fig. 6(c), one notes that $[T(\tau) - T_0]/T_0$ amounts to a few hundredths (~ 0.02), which is significantly lower than the

expectation for a cluster glass (i.e., a few tenths) [31]. The same conclusion can be drawn by considering the Mydosh parameter $[\Delta(\ln T_f)/\Delta(\ln f)]$ which presently gets a quite small value (~ 0.004) consistent with a spin glass (SG) but not with a cluster glass (CG) [32]. In the end, the presence of a peak in $\chi_{2\omega}$ indicates that the prepeak at $T_p(f)$ cannot be related to a SG behavior, while a description in terms of CG is ruled out by a quantitative analysis of the spin dynamics.

V. DISCUSSION

The transient dynamical response taking place just above T_N in $\text{Sr}_2\text{Ca}_2\text{CoMn}_2\text{O}_9$ is the central issue of the present paper. First of all, let us specify that we could not find any previous report of similar behavior in the literature about spin-chain compounds on triangular lattices. On the other hand, such a prepeak is not restricted to $\text{Sr}_2\text{Ca}_2\text{CoMn}_2\text{O}_9$, since it was observed in the $\text{Sr}_{4-x}\text{Ca}_x\text{CoMn}_2\text{O}_9$ compounds with $x > 1.5$. In all cases, a frequency-dependent peak T_p emerges in between the onset of LRO at $T_N(x)$ and a slightly higher temperature $T^*(x)$ marking the rise of a spontaneous magnetization (see Supplemental Material [21]). It turns out that these two characteristic temperatures (T_N and T^*) appear concomitantly when x is varied, and they increase together when increasing the couplings via chemical pressure, demonstrating that they are closely linked to each other [21].

The first issue to be addressed is the nature of the magnetic order taking place at T_N . $\text{Sr}_2\text{Ca}_2\text{CoMn}_2\text{O}_9$ exhibits Ising chains distributed on a triangular lattice, and which interact via AF nn interchain coupling, a situation known to often trigger the onset of a PDA state [6]. The PND pattern was found to be consistent with such a PDA state (see Supplemental Material [21]). The achievement of a PDA state is also consistent with the physical properties: (i) The heat capacity exhibits at T_N a peak of moderate intensity (as expected owing to the partial nature of the ordering in PDA); (ii) when cooling below T_N , the magnetization shows an increase in low fields (ascribable to the easy polarization of the incoherent chains) which is replaced by a peak in larger fields (consistent with the fact that AF coupling of two-thirds of the chains leads to a reduced global magnetization compared to the paramagnetic response).

The PDA model was originally developed for strictly identical spin chains. Phenomena of interexchange between the three magnetic sublattices can thus take place and contribute to destabilize this ordering [33]. In this regard, it deserves to be noted that the structural partition into A and B chains encountered in $\text{Sr}_2\text{Ca}_2\text{CoMn}_2\text{O}_9$ (see Fig. 1) is favorable to the achievement of a PDA state. A similar remark was previously emphasized by Adachi *et al.* in the case of RbFeBr_3 [34].

To understand the anomaly taking place above T_N , a key issue is the nature of the phenomenon occurring at T^* . Experimentally T^* is characterized by the following features: (a) rise of an M_{spont} , (ii) emergence of nonlinearity in the magnetic response, (iii) appearance of peaks in the second and third harmonics; and (iv) hysteretical $M(H)$ curves. This temperature also marks the vanishing of the remanent magnetization when increasing temperature (see Supplemental Material [21]). This set of features points to the formation of correlated magnetic

units showing a net magnetization at T^* . Since both the PND and $C(T)$ data do not show any signature of LRO in this T range, the transition at T^* should be ascribed to the formation of SRO units having a FM-like response. We emphasize that the abrupt changes in physical properties seen at T^* support the onset of a real magnetic order, even if it develops only over short lengths (e.g., clusters or domains).

A very important feature of the SRO taking place at T^* is that it seems to involve only a part of the spins. This is visible in the $M(H)$ curves, which look like the superimposition of a FM-like response onto a paramagnetic (PM) background. Such a dual character of the magnetic response is also visible on the susceptibility curves, in that the peak at $T_p(f)$ curves clearly appears to be superimposed onto a PM background. One observes that the SRO contribution is prominent on magnetic data for low-field values, i.e., for ac data as well as dc data when recorded in small H . When increasing the field, the signatures of T^* are rapidly washed out. Accordingly, the magnetic signatures rising at T^* can be ascribed to the existence of a small M_{spont} (originating from FM-like SRO) that coexists with a PM response involving the greatest part of the spins.

We have previously noted that the spin-chain system of $\text{Sr}_2\text{Ca}_2\text{CoMn}_2\text{O}_9$ is not an ideal triangular lattice, and should rather be regarded as a centered honeycomb lattice. This topology was investigated in theoretical works along the 90s [35], motivated by experimental realizations of such centered honeycomb lattices in a particular class of the ABX_3 compounds (the so-called KNiCl_3 family) [36]. The compound which is the closest to ours is RbCoBr_3 : it exhibits a pronounced Ising character and three subclasses of chains with relative shiftings equal to 0, $+\delta$, and $-\delta$, like for $\text{Sr}_2\text{Ca}_2\text{CoMn}_2\text{O}_9$. Experimentally, RbCoBr_3 was found to undergo a LRO from a PM to a PDA state, but without any evidence of pretransitional features [37].

In the ABX_3 materials, it must be emphasized that one can encounter shifting along the c axis between neighboring chains, but the intrachain distances along all these chains remain identical. What is quite unique in our compound is that it displays two different types of chains (A and B): these chains are made of the same spins, arranged with the same sequence, but some of the interdistances between them are modified. This introduces a difference on some of the intrachain couplings (J_2 and J_4) that will in turn induce modifications in the effective ferromagnetic coupling between successive ($\uparrow\downarrow\uparrow$) units along the chain, leading to $J_A \neq J_B$ [38]. Even though one cannot anticipate the amplitude of ($J_A - J_B$) nor even its sign, this dissymmetry can have a non-negligible impact on the ordering process. As for the interchain couplings, one can expect that $j_{\text{BB}} < j_{\text{AB}}$ owing to the less direct supersuperexchange links between spins of adjacent B chains (in the present paper, positive coupling parameters correspond to AF interactions).

To the best of our knowledge, there are no theoretical predictions on centered honeycomb lattices with two different intrachain couplings. Considering that the magnetic ordering between chains is governed by a combination of intrachain and interchain couplings [39], we naively anticipate that the situations should be different for the A and B chains: in first approximation, the ordering of A chains involves the

couplings J_A and j_{AB} , whereas that of the B chains rather involve J_B , j_{AB} , and j_{BB} .

On this basis, let us suggest a qualitative scenario susceptible to account for the presence of a pretransitional regime in $\text{Sr}_2\text{Ca}_2\text{CoMn}_2\text{O}_9$. As the temperature is decreased toward T^* , the spin system prepares to enter the PDA state: the sublattice made of the B chains tends toward an AF arrangement (i.e., alternation of chains with a net magnetization either up or down), while each A chain undergoes antagonist interactions from its six nn B chains. In the usual case where $J_A = J_B$, the A chains remain PM till they transform to incoherent at T_N . Assuming that the combination of intra- and interchain couplings is stronger for the A chains than for the B ones, ordering might start developing along these A chains above the onset of PDA, i.e., at a slightly higher temperature assumed to be T^* . Let us recall that the energetically most favorable arrangement along the chains [$\text{Co}^{2+}(\uparrow) - \text{Mn}^{4+}(\downarrow) - \text{Mn}^{4+}(\uparrow)$] can be seen as an effective FM coupling between ferrimagnetic ($\uparrow\downarrow\uparrow$) units [17]. The growth of FM-like correlations along the A chains is impeded by the AF coupling with the B chains. This can limit the ordering along the A chains to segments oriented either up or down, in order to maintain a zero net magnetization. When the temperature is decreased below T^* , these 1D FM-like segments could exhibit specific dynamical signature leading to the susceptibility peak at $T_p(f)$. As T is further decreased, the B chains eventually reach the conditions to be ordered too, leading to the achievement of PDA state at T_N .

Note that the above-described 1D SRO along the A chains is prone to be polarized by the application of a magnetic field. A net magnetization can thus be induced at T^* in low fields, associated with a dissymmetry between up and down segments, resulting from displacements of domain walls between them. This is thus consistent with the rise of an M_{spont} at T^* . Moreover, the signature of this 1D SRO is expected to vanish when the applied field is large enough to polarize both the A and B chains in the PM state.

On this basis, the hysteresis in low-field magnetization can be ascribed to energy barriers affecting the domain wall displacement. ac susceptibility data are also expected to be impacted by the mobility of such domain walls along the chains. Owing to a blocking phenomenon, one observes that the $\chi'(T)$ peak shifts toward lower temperature as the frequency is decreased, allowing its height to increase spectacularly (Fig. 3). We emphasize that one is dealing with an unusual type of blocking since the interchain interactions take substantial part in the slowdown of spin dynamics [40,41]. It is likely the reason why the spin relaxation does not follow an Arrhenius behavior but rather a VF law with a T_0 closely related to T_N .

VI. CONCLUSION

This paper reports the oxide $\text{Sr}_2\text{Ca}_2\text{CoMn}_2\text{O}_9$ which is made of Ising spin chains distributed on a triangular lattice. However, this compound exhibits two peculiarities which make it depart from a simple triangular lattice: first, it contains two types of chains (A and B) differing by their intrachain Co-Mn distances, and whose spatial arrangement draws a centered honeycomb lattice; second, there are global

shiftings by $\pm 1.9 \text{ \AA}$ along the c axis (direction of the chains) between the A and B chains. The competition between the nn- and nnn intrachain couplings favors a ferrimagnetic response along each chain, while the coupling between nn chains is AF. The LRO taking place at $T_N \sim 28.3 \text{ K}$ is found to be consistent with a PDA state in which the A chains remain incoherent.

A peculiar spin dynamics is observed within a pretransitional regime between T_N and a characteristic temperature T^* ($\sim 32.5 \text{ K}$). We suggest that it corresponds to a transient regime along the setting up of the PDA state, whose origin relies on the difference between the A and B chains. Assuming that the A chains are more prone to order than the B ones (owing to a more favorable combination of intrachain and interchain couplings), SRO can develop along these A chains (at T^*) a few kelvin above the LRO (at T_N). As a consequence, this generates a narrow T range ($T_N < T < T^*$) where the magnetic response is strongly impacted by the dynamics of such 1D correlated segments. The energy barriers involved

in this dynamics combine not only easy-axis anisotropy and intrachain couplings but also the interchain interactions.

We fully recognize that more work is required to elucidate the exact nature of the susceptibility peak at $T_p(f)$ in $\text{Sr}_2\text{Ca}_2\text{CoMn}_2\text{O}_9$. From an experimental point of view, local probes such as muon spin relaxation or nuclear magnetic resonance would be highly welcome. We also hope that the present work could trigger theoretical studies addressing the peculiar type of spin lattice encountered in this study, i.e., a centered honeycomb lattice involving not only different interchain couplings but also different intrachain couplings.

ACKNOWLEDGMENTS

We acknowledge financial support from the Région Normandie (PhD thesis of N.S.) and from the University of Caen (Visiting professor position for Md.M.S.).

-
- [1] *Frustrated Spin Systems*, edited by H. T. Diep (World Scientific, Singapore, 2004); R. Moessner and A. P. Ramirez, *Phys. Today* **59**(2), 24 (2006); L. Balents, *Nature (London)* **464**, 199 (2010); *Introduction to Frustrated Magnetism*, Springer Series in Solid-State Sciences 164, edited by C. Lacroix, P. Mendels, and F. Mila (Springer, Berlin, 2011).
- [2] G. H. Wannier, *Phys. Rev.* **79**, 357 (1950).
- [3] J. Stephenson, *J. Math. Phys.* **11**, 420 (1970); *Can. J. Phys.* **48**, 2118 (1970); O. Nagai, S. Miyashita, and T. Horiguchi, *Phys. Rev. B* **47**, 202 (1993); W.-M. Zhang, W. M. Saslow, M. Gabay, and M. Benakli, *ibid.* **48**, 10204 (1993); R. R. Netz, *ibid.* **48**, 16113 (1993); A. Lipowski, T. Horiguchi, and D. Lipowska, *Phys. Rev. Lett.* **74**, 3888 (1995); M. F. Collins and O. Petrenko, *Can. J. Phys.* **75**, 605 (1997); Y. Jiang and T. Emig, *Phys. Rev. B* **73**, 104452 (2006).
- [4] N. Achiwa, *J. Phys. Soc. Jpn.* **27**, 561 (1969).
- [5] W. B. Yelon, D. E. Cox, and M. Eibschütz, *Phys. Rev. B* **12**, 5007 (1975); M. Mekata and K. Adachi, *J. Phys. Soc. Jpn.* **44**, 806 (1978); H. Yoshizawa and K. Hirakawa, *ibid.* **46**, 448 (1980).
- [6] M. Mekata, *J. Phys. Soc. Jpn.* **42**, 76 (1977).
- [7] J. Darriet and M. A. Subramanian, *J. Mater. Chem.* **5**, 543 (1995); J. M. Perez-Mato, M. Zakhour-Nakhl, F. Weill, and J. Darriet, *ibid.* **9**, 2795 (1999); K. E. Stitzer, J. Darriet, and H.-C. zur Loye, *Curr. Opin. Solid State Mater. Sci.* **5**, 535 (2001).
- [8] H.-C. zur Loye, Q. Zhao, D. E. Bugaris, and W. M. Chance, *CrystEngComm* **14**, 23 (2012).
- [9] H. Kageyama, K. Yoshimura, K. Kosuge, H. Mitamura, and T. Goto, *J. Phys. Soc. Jpn.* **66**, 1607 (1997).
- [10] S. Aasland, H. Fjellvåg, and B. Hauback, *Solid State Commun.* **101**, 187 (1997); A. Maignan, C. Michel, A.-C. Masset, C. Martin, and B. Raveau, *Eur. Phys. J. B* **15**, 657 (2000); V. Hardy, S. Lambert, M. R. Lees, and D. McK. Paul, *Phys. Rev. B* **68**, 014424 (2003); E. V. Sampathkumaran, N. Fujiwara, S. Rayaprol, P. K. Madhu, and Y. Uwatoko, *ibid.* **70**, 014437 (2004); V. Hardy, M. R. Lees, O. A. Petrenko, D. McK. Paul, D. Flahaut, S. Hébert, and A. Maignan, *ibid.* **70**, 064424 (2004); V. Hardy, D. Flahaut, M. R. Lees, and O. A. Petrenko, *ibid.* **70**, 214439 (2004); H. Wu, M. W. Haverkort, Z. Hu, D. I. Khomskii, and L. H. Tjeng, *Phys. Rev. Lett.* **95**, 186401 (2005); V. Hardy, D. Flahaut, R. Frésard, and A. Maignan, *J. Phys.: Condens. Matter* **19**, 145229 (2007); S. Agrestini, L. C. Chapon, A. Daoud-Aladine, J. Schefer, A. Gukasov, C. Mazzoli, M. R. Lees, and O. A. Petrenko, *Phys. Rev. Lett.* **101**, 097207 (2008); S. Agrestini, C. Mazzoli, A. Bombardi, and M. R. Lees, *Phys. Rev. B* **77**, 140403(R) (2008).
- [11] S. Niitaka, K. Yoshimura, K. Kosuge, M. Nishi, and K. Kakurai, *Phys. Rev. Lett.* **87**, 177202 (2001).
- [12] E. V. Sampathkumaran and A. Niazi, *Phys. Rev. B* **65**, 180401 (2002); V. Hardy, M. R. Lees, A. Maignan, S. Hébert, D. Flahaut, C. Martin, and D. McK. Paul, *J. Phys.: Condens. Matter* **15**, 5737 (2003); M. Loewenhaupt, W. Schäfer, A. Niazi, and E. V. Sampathkumaran, *Europhys. Lett.* **63**, 374 (2003); H. Wu, Z. Hu, D. I. Khomskii, and L. H. Tjeng, *Phys. Rev. B* **75**, 245118 (2007); T. Burnus, Z. Hu, H. Wu, J. C. Cezar, S. Niitaka, H. Takagi, C. F. Chang, N. B. Brookes, H.-J. Lin, L. Y. Jang, A. Tanaka, K. S. Liang, C. T. Chen, and L. H. Tjeng, *ibid.* **77**, 205111 (2008).
- [13] Y. J. Choi, H. T. Yi, S. Lee, Q. Huang, V. Kiryukhin, and S.-W. Cheong, *Phys. Rev. Lett.* **100**, 047601 (2008); H. Wu, T. Burnus, Z. Hu, C. Martin, A. Maignan, J. C. Cezar, A. Tanaka, N. B. Brookes, D. I. Khomskii, and L. H. Tjeng, *ibid.* **102**, 026404 (2009); Y. J. Jo, S. Lee, E. S. Choi, H. T. Yi, W. Ratcliff II, Y. J. Choi, V. Kiryukhin, S.-W. Cheong, and L. Balicas, *Phys. Rev. B* **79**, 012407 (2009); V. Kiryukhin, S. Lee, W. Ratcliff II, Q. Huang, H. T. Yi, Y. J. Choi, and S.-W. Cheong, *Phys. Rev. Lett.* **102**, 187202 (2009); T. Lancaster, S. J. Blundel, P. J. Baker, H. J. Lewtas, W. Hayes, F. L. Pratt, H. T. Yi, and S.-W. Cheong, *Phys. Rev. B* **80**, 020409(R) (2009).
- [14] A. El Abed, E. Gaudin, J. Darriet, and M.-H. Whangbo, *J. Solid State Chem.* **163**, 513 (2002).
- [15] M. Hernando, K. Boulahya, M. Parras, A. Varela, J. M. González-Calbet, and J. L. Martínez, *Chem. Mater.* **14**, 4948 (2002); G. V. Bazuev, V. N. Krasil'nikov, and D. G. Kellerman,

- J. Alloys. Compd.* **352**, 190 (2003); C. A. Moore and P. D. Battle, *J. Solid State Chem.* **176**, 88 (2003).
- [16] K. Boulahya, M. Parras, J. M. Gonzalez-Calbet, and J. L. Martinez, *Chem. Mater.* **15**, 3537 (2003); K. Boulahya, M. Hernando, M. Parras, and J. M. Gonzalez-Calbet, *ibid.* **17**, 1620 (2007).
- [17] Md. Motin Seikh, V. Caignaert, O. Perez, B. Raveau, and V. Hardy, *Phys. Rev. B* **95**, 174417 (2017).
- [18] See, for a review, C. Coulon, H. Miyasaka, and R. Clérac, *Struct. Bond.* **122**, 163 (2006); C. Coulon, V. Pianet, M. Urdampilleta, and R. Clérac, *ibid.* **164**, 143 (2014).
- [19] See, for a review, D. Gatteschi, R. Sessoli, and J. Villain, *Molecular Nanomagnets* (Oxford University Press, Oxford, 2006) and J. M. Frost, K. L. M. Harriman, and M. Murugesu, *Chem. Sci.* **7**, 2470 (2016).
- [20] Md. M. Seikh, V. Caignaert, O. Perez, B. Raveau, and V. Hardy, *J. Mater. Chem. C* **6**, 3362 (2018).
- [21] See Supplemental Material at <http://link.aps.org/supplemental/10.1103/PhysRevB.98.144414> for details on the structural data, the derivation of $\tau_c(T)$ from $\chi''(T, f)$, additional physical properties and the impact of x on the pretransitional regime within the series $\text{Sr}_{4-x}\text{Ca}_x\text{CoMn}_2\text{O}_9$.
- [22] R. Frésard, C. Laschinger, T. Kopp, and V. Eyert, *Phys. Rev. B* **69**, 140405(R) (2004); L. C. Chapon, *ibid.* **80**, 172405 (2009); Y. Kamiya and C. D. Batista, *Phys. Rev. Lett.* **109**, 067204 (2012).
- [23] S. Gómez-Coca, D. Aravena, R. Morales, and E. Ruiz, *Coord. Chem. Rev.* **289–290**, 379 (2015); Y. Peng, T. Bodenstein, K. Kink, V. Mereacre, C. E. Anson, and A. K. Powell, *Phys. Chem. Chem. Phys.* **18**, 30135 (2016).
- [24] Y.-Y. Zhu, C. Cui, Y.-Q. Zhang, J.-H. Jia, X. Guo, C. Gao, K. Qian, S.-D. Jiang, B.-W. Wang, Z.-M. Wang, and S. Gao, *Chem. Sci.* **4**, 1802 (2013); V. V. Novikov, A. A. Pavlov, Y. V. Nelyubina, M.-E. Boulon, O. A. Varzatskii, Y. Z. Voloshin, and R. E. P. Winpenny, *J. Am. Chem. Soc.* **137**, 9792 (2015).
- [25] Y. Zhang, H. J. Xiang, and M.-H. Whangbo, *Phys. Rev. B* **79**, 054432 (2009).
- [26] Such a small shift by ~ 0.5 K can be ascribed to the fact that T^* has been derived from data recorded in a still lower field (~ 1.5 Oe).
- [27] T. Sato and Y. Miyako, *J. Phys. Soc. Jpn.* **51**, 1394 (1981); L. P. Lévy and A. T. Ogielski, *Phys. Rev. Lett.* **57**, 3288 (1986); M. Mito, M. Ogawa, H. Deguchi, M. Yamashita, and H. Miyasaka, *J. Appl. Phys.* **107**, 124316 (2010).
- [28] K. S. Cole and R. H. Cole, *J. Chem. Phys.* **9**, 341 (1941).
- [29] Let us emphasize, however, that the discrepancy remains moderate (~ 0.45 K). It is well visible in Fig. 6 because of both the sharpness of the transition and the steepness of the divergence of $\tau_c(T)$.
- [30] S. Shtrikman and E. P. Wohlfarth, *Phys. Lett. A* **85**, 467 (1981); J. Souletie and J. L. Tholence, *Phys. Rev. B* **32**, 516 (1985); W. M. Saslow, *ibid.* **37**, 676 (1988).
- [31] D. Fiorani, J. Tholence, and J. L. Dormann, *J. Phys. C: Solid State Phys.* **19**, 5495 (1986); S. Mukherjee, R. Ranganathan, P. S. Anilkumar, and P. A. Joy, *Phys. Rev. B* **54**, 9267 (1996).
- [32] J. A. Mydosh, *Spin-Glasses: An Experimental Introduction* (Taylor and Francis, London, 1993).
- [33] S. Fujiki, K. Shutoh, Y. Abe, and S. Katsura, *J. Phys. Soc. Jpn.* **52**, 1531 (1983); F. Matsubara and S. Inawashiro, *ibid.* **53**, 4373 (1984).
- [34] K. Adachi, K. Takeda, F. Matsubara, M. Mekata, and T. Haseda, *J. Phys. Soc. Jpn.* **52**, 2202 (1983).
- [35] H. T. Diep, M. Debauche, and H. Giacomini, *Phys. Rev. B* **43**, 8759 (1991); M. L. Plumer, A. Caillé, and H. Kawamura, *ibid.* **44**, 4461 (1991); M. E. Zhitomirsky, O. A. Petrenko, and L. A. Prozorova, *ibid.* **52**, 3511 (1995).
- [36] K. Yamanaka, Y. Nishiwaki, K. Iio, T. Mitsui, T. Tojo, and T. Atake, *J. Therm. Anal. Calorim.* **70**, 371 (2002).
- [37] Y. Nishiwaki, T. Nakamura, A. Oosawa, K. Kakurai, N. Todoroki, N. Igawa, Y. Ishii, and T. Kato, *J. Phys. Soc. Jpn.* **77**, 104703 (2008).
- [38] The (intrachain) effective FM coupling between adjacent $\text{Co}(\uparrow)\text{-Mn}(\downarrow)\text{-Mn}(\uparrow)$ units can be evaluated by considering (half of) the difference in interaction energy between the configurations $(\uparrow\downarrow\uparrow)\text{-}(\uparrow\downarrow\uparrow)$ and $(\uparrow\downarrow\uparrow)\text{-}(\downarrow\uparrow\downarrow)$. This leads to $J = J_2 - J_3 - J_4$.
- [39] H. Shiba, *Prog. Theor. Phys.* **64**, 466 (1980).
- [40] D. A. Pejakovic, J. L. Manson, J. S. Miller, and A. J. Epstein, *Phys. Rev. Lett.* **85**, 1994 (2000).
- [41] M. Evangelisti, J. Bartolomé, L. J. de Jongh, and G. Filoti, *Phys. Rev. B* **66**, 144410 (2002).